JOURNAL OF GEOPHYSICAL RESEARCH, VOL. 106, NO. B1, PAGES 803–817, JANUARY 10, 2001

Salt tectonics as a self-organizing process: A reaction, transport, and mechanics model

K. Tuncay and P. Ortoleva
Laboratory for Computational Geodynamics, Department of Chemistry, Indiana University, Bloomington

Abstract. Salt tectonics is placed within the theory of nonlinear dynamical systems. Features such as waves, diapirs, and tears are viewed as natural consequences of the symmetry breaking instabilities and related self-organized dynamics of the deforming salt body coupled to the reaction, transport, and mechanics of the surrounding sediments. The fundamental nonlinearities are in the surrounding-rock and salt rheology. Our findings are based on a coupled RTM model simulated using finite element techniques. The centerpiece of the rheology of both rocks and salt is a nonlinear incremental stress formulation that integrates poroelasticity, continuous irreversible mechanical deformation (with yield behavior), pressure solution, and fracturing. In contrast to previously presented studies, in our approach the descriptive variables of all solid and fluid phases (stress, velocity, concentrations, etc.) and porous media (texture, i.e., volume fractions, composition, etc.) are solved from RTM equations accounting for interactions and interdependencies between them. The role of the coupling between the spatial distribution of sediment input rate and diapir growth and stalling is examined as is the creation of an array of salt tectonic minibasins.

1. Introduction

While salt tectonics has long been recognized as a key process in basin evolution and in particular in the context of petroleum reservoir location and characteristics, most studies have not addressed the complexities caused by the interplay of salt deformation with the other basin reaction, transport, and mechanical (RTM) processes. In this paper, we focus on the role of nonlinearity and examine the interplay between the coupling of salt deformation with sedimentation and the myriad of other RTM processes operating in a basin. We address these issues using a unique finite element model that integrates a wide range of coupled RTM processes.

In the present view, salt tectonics features are the consequences of a symmetry breaking of the idealized planar state of a salt layer overlain and underlain by other horizontal sediments. Small disturbances in the transitional invariance of the system in the horizontal directions can be amplified by the RTM processes into wave, diapir, and more complex features. This view has been successful in understanding a wealth of phenomena in geological systems [see *Ortoleva,* 1990, 1994a, 1994b, 1998; *Turcotte*, 1992; F. Renard and P. Ortoleva, manuscript in preparation, 2000] and in the wider context of self-organizing physical and chemical systems [*Nicolis and Prigogine*, 1977].

The controversy as to the physical laws underlying salt tectonics and hence, in our view the aforementioned self-organization, still has not been completely resolved [*Koen,* 1993; *Taylor,* 1995]. We believe that this is because while one can rather easily conjecture a variety of mechanisms, it is likely a quantitative question as to which one is dominant in a given geological context. Furthermore, experience gained over the past 3 decades in nonlinear dynamical systems shows that they often behave in rather unexpected ways. Our solution to this dilemma is to study salt tectonics using a comprehensive, multiprocess simulator. Our simulator accounts for a range of the conjectured mechanisms, allowing us to weigh the relative importance of the various factors quantitatively. In such an approach, one may test the relative importance of the various factors and furthermore evaluate the degree to which they reinforce or inhibit one another.

Because of its relatively low shear viscosity, salt rheology has been the subject of many experimental studies [e.g., *Wawersik,* 1985; *Aubertin et al.*, 1994; *De Las Cuevas,* 1997; *Carter et al.*, 1993; *Mazeriegos et al.*, 1996; *Van Keken et al.*, 1993; *Munson and Dawson,* 1984]. Thus as salt and surrounding-rock deformation are strongly coupled, the rheologic challenge in unraveling salt tectonics must focus on the evolving rheology of the surrounding rocks.

Wawersik [1985] measured steady state salt creep rates and activation parameters at low temperature and low strain rates. *Aubertin et al.* [1994] investigated kinematic hardening in salt on the basis of a triaxial compression tests and proposed procedures that can be used to isolate kinematic and isotropic components. The pore structure of rock salt was studied by *De Las Cuevas* [1997], who reported porosities in the range of 0.97 to 3.09%. De Las Cuevas also studied the pore sizes and concluded that pores may be present as macropores, micropores, and infrapores, and that porosity is mainly associated with the existence of a well-developed microporous system. Another attempt to formulate salt rheology was presented by *Carter et al.* [1993], who proposed two expressions for the total rate of strain for high stress-high strain rate and low stress-low strain rate cases. More generally, laboratory experiments on salt and other lithologies have shown that the total rate of strain can be expressed as a sum of rates of various deformation processes such as elastic strain, plastic strain, and primary and secondary creep.

Paper number 2000JB900107.
0148-0227/01/2000JB900107$09.00

Laboratory analog models have been used to generate new concepts that can be utilized to interpret observations [*Vendeville and Jackson,* 1992; *Weijemars et al.,* 1993; *Ge et al.,* 1997; *Jackson and Vendeville,* 1994; *Jackson et al.,* 1988]. Among the emerging concepts one can note the role of thin-skinned extension in initiating and promoting diapirism, the initiation of salt diapirism by regional extension, the importance of progradation as a trigger for salt tectonics, and the interaction between salt flow and overburden faulting during extension. Most of these concepts are yet to be modeled and tested by a comprehensive numerical salt tectonics simulator.

Although there is a vast number of observations of salt structures [*Jackson and Talbot,* 1986, 1991; *Seni and Jackson,* 1984; *Cobbold,* 1993], there are only a few attempts to numerically simulate them. Moreover, previous simulators are two-dimensional, and both salt and sediment are treated as bulk materials; that is, fluid flow through the pores and its influence on effective stress are ignored. None of these models account for the evolving rheology of the sediments due to diagenesis, mechanical processes, petroleum generation, and the changing thermal regime. Therefore existing salt tectonics simulators do not have the sufficient comprehensiveness that can assist the salt related exploration.

Daudre and Cloetingh [1994] presented a two-dimensional analysis based on Stokes flow. In this approach both sediment and salt were treated as nonlinear viscous fluids. A Drüker-Prager criterion was adopted to model the inception of brittle deformation. The density of sediment was calculated based on a pressure-dependent porosity. An updated Lagrangian formulation was used to simulate large deformations. They showed that extension combined with salt rheology favors salt diapirism. *Van Keken et al.* [1993] obtained the effective rock salt viscosity by adding dislocation creep and pressure solution creep. The effective salt viscosity was allowed to depend on temperature, strain rate, and grain size. Pressure solution dominated the salt motion. Sediment density was taken as a function of depth. With these assumptions, they performed a sensitivity analysis for the effect of overlying sediment viscosity. Their results showed that the sediment viscosity/salt viscosity ratio is an important factor in determining salt motion and geometry. Another two-dimensional model was developed by *Mazeriegos et al.* [1996] on the basis of Stokes flow. They used two different salt rheologies: a dislocation-creep power law and a fluid-assisted creep law. The functional form of the salt rheology depended on grain size. Although they used a rather complex rheology for salt, sediment viscosity was taken to be constant. They showed that their fluid-assisted creep law results in faster salt motion. They concluded that a better understanding of salt diapirism requires a better characterization of surrounding rock rheology. A two-dimensional study was presented by *Schultz-Ela et al.* [1994], who used the commercial program GEOSIM-2D for their numerical modeling. Salt was treated as a viscoelastic material, whereas sediment was modeled with an elastoplastic rheology. Plastic yield was determined with a Drüker-Prager criterion.

In all of these studies the results were limited to two dimensions. However, the most crucial difficulty is that they are limited to the deformation of bulk media. In other words, they do not employ the theory of composite porous media. In composite environments the velocity, stress, and other descriptive variables of solid and fluid phases show very different time history and spatial distributions. For example the velocity and stress tensor of solid and fluid phases are very distinct. Therefore, although approximation of such a complicated composite medium by an equivalent bulk medium may give some information, it cannot have the predictive power of a composite model.

The differences between our model and those mentioned above are as follows.

1. For the concept of composite media, in contrast to previous studies, our approach coevolves the descriptive variables of all solid and fluid phases (stress, velocity, concentrations, etc.) and variables describing the texture of the porous medium (i.e., volume fractions, mineralogy, grain size, and porosity) via RTM equations accounting for interactions and interdependencies between them.

2. Incremental stress rheology integrates poroelasticity, viscous flow with yield behavior, fracturing, and pressure solution. In most studies, salt and sediment are considered as nonlinear Newtonian fluids ignoring the effects of elasticity and fracturing [*Ortoleva,* 1994a, 1998; *Tuncay et al.,* 2000a, 2000b, 2000d; *Ortoleva et al.,* 1997].

3. For faulting, we use the Drüker-Prager criterion to signal failure and to evaluate the rheologic properties of the failed medium. However, the nonlinear shear viscosity is obtained from coevolving texture variables such as rock "competency," mineral composition, grain size distribution, and porosity. In our model, the competency of a rock is a measure of the integration of grain-grain contacts. It has memory, i.e., it depends on the history of failure through its determination as the solution of a time-differential equation [*Tuncay et al.,* 2000c].

4. We have developed a fracture mechanics model based on the stress tensor, fluid pressure, and rock texture variables. Since previous models are limited to simulating the behavior of bulk materials, they cannot be used to predict or understand tensile fractures which contribute to the tensorial rock permeability [*Tuncay et al.,* 2000a, 2000b].

5. Salt deformation and fluid flow should be solved simultaneously for single and multiphase flow in order to understand the interplay of salt motion and fluid migration. The presence of seals and overpressured and underpressured compartments can enhance or suppress salt motion, an effect that is not accounted for in other models.

6. As a natural consequence of the availability of our multiphase flow solver, generation and migration of petroleum can be studied in association with salt motion.

7. We use coupling of sedimentation and salt motion, while most studies ignore sedimentation and erosion. Our numerical technique accounts for nonuniform sedimentation or erosion associated with salt motion-induced surface topology.

8. While salt rheology is fairly well approximated by existing laws, the rheology of the evolving sediment dictates the overall salt motion. Therefore a model that can evolve sediment properties including poroelasticity and viscosity coefficients is required for capturing the time dependence and spatial distribution of salt bodies.

The rock and salt rheology and the multiphase flow model used in this study are outlined in section 2. The nature of our sedimentation modeling is discussed in section 3, where the interplay of salt motion and sedimentation is reviewed. In section 4 the numerical approach is briefly reviewed. In section 5 we present simulation results, while conclusions and potential applications for petroleum exploration and production are reviewed in section 6.

2. Salt and Rock Rheology, Textural Coupling, and Fluid Flow

2.1. Incremental Stress Rheology

When salt migrates in the subsurface, it must do so in coordination with the deformation of the neighboring sediments. If the latter are rigid, salt motion is clearly inhibited. Thus in a cool basin (salt viscosity is high) with a high rate of sedimentation, salt diapirism is

repressed as the overlying rocks can become highly lithified before salt deforms appreciably. However, in a hot basin, salt diapirism can keep in step with sedimentation and the salt waves and diapirs can rise continuously.

More generally, salt tectonics is the result of a number of competing effects. Increased temperature and decreased sediment grain size promote the rate of lithification although increased temperature also enhances pore fluid overpressuring that retards compaction/lithification. What is needed to address these factors is a rock rheology that changes dynamically due to diagenesis and mechanical processes. Such complex interactions between rock properties, changing rock texture and mineralogy, and salt deformation have not been included in earlier models.

In our approach, we coevolve rock texture and rock deformation, coupling them through the texture dependence of rheological parameters and the stress dependence of the rate of change of texture. This texture-deformation coupling is the basis of recent theories of a number of phenomena, including (1) metamorphic layering, (2) stylolites and banded compaction/cementation alternations, and (3) gouge/fault inner structure [see *Ortoleva,* 1994a, 1998; *Dewers and Ortoleva,* 1989, 1990a, 1990b, 1990c, 1990d, 1992, 1994a, 1994b; F. Renard and P. Ortoleva, manuscript in preparation, 2000], and underlies our basin deformation modeling approach [*Tuncay, Park et al.*, 2000a, 2000b, 2000c; *Ortoleva,* 1998; *Ortoleva et al.*, 1997]. As salt diapirism depends on the relative timing of putative salt movement and rock lithification, we believe that texture-stress coupling must be part of any quantitative or qualitative salt tectonics model.

The strongly coupled nature of the basin deformation problem is captured using an incremental stress rheology [*Rice*, 1975]. The specific rheology used in our simulator integrates most strain mechanisms believed to operate in a basin. It has the form [*Tuncay et al.*, 2000a, 2000c; *Ortoleva,* 1994a, 1998]

$$\dot{\varepsilon}_{ii'} = \dot{\varepsilon}^{el}_{ii'} + \dot{\varepsilon}^{vp}_{ii'} + \dot{\varepsilon}^{fr}_{ii'} + \dot{\varepsilon}^{ps}_{ii'} . \tag{1}$$

Here $\dot{\varepsilon}_{ii'}$ is the net rate of strain, while the terms on the right give the contributions from four processes: poroelasticity (el), continuous viscoplastic (vp), pressure solution (ps), and fracturing (fr). In this study, we consider poroelasticity, viscosity, and fracturing. One expects that $\dot{\varepsilon}^{j}_{ii'}$ (where j is poroelasticity, viscosity, pressure solution, fracturing, etc.) should in general depend on all the aforementioned variables (σ,Θ,p,c) as well as absolute temperature T. With this,

$$\dot{\varepsilon}_{ii'} = \sum_{j=1}^{N_q} \dot{\varepsilon}^{j}_{ii'}(\Theta,\sigma,p,c.T) , \tag{2}$$

where σ is the total stress tensor, p is the wetting phase fluid pressure, T is the temperature, and Θ is the rock texture. The texture Θ represents a set of variables characterizing the mineralogy, shape, size, orientation, and packing of the grains, as well as the fracture length, aperture, number density, and orientation statistics. The dependency of the $\dot{\varepsilon}^{j}_{ii'}$ on the indicated state variables may be nonlocal in time. For example, in the case of poroelasticity, $\dot{\varepsilon}^{ps}_{ii'}$ depends on the time derivative of effective stress. Therefore the $\dot{\varepsilon}^{j}_{ii'}$ may be functionals of their arguments that can, in principle, sample the state variables in some finite volume of space-time.

The total rate of strain $\dot{\varepsilon}_{ii'}$ is defined via

$$\dot{\varepsilon}_{ii'} = \frac{1}{2}\left(\frac{\partial u_i}{\partial x_{i'}} + \frac{\partial u_{i'}}{\partial x_i} \right). \tag{3}$$

The six independent components of the symmetric second rank tensor equation (3) must be supplemented with three additional equations so that the three deformation velocity components $(\mathbf{u}=u_1,u_2,u_3)$ can be determined. The required condition arises from force balance:

$$\sum_{i'=1}^{3} \frac{\partial \sigma_{ii'}}{\partial x_{i'}} + f_i = 0 \tag{4}$$

for body force f_i, which, for gravity, is given by

$$f_i = g\rho_m \delta_{i3} . \tag{5}$$

Here g is the gravitational acceleration, ρ_m is the mass density, and the three-direction is upward.

Once the rock velocity field is determined, porosity can be calculated from the mass balance of solids assuming incompressible solid grains:

$$\frac{D\phi}{Dt} = (1-\phi)\nabla\cdot\mathbf{u}, \tag{6}$$

where ϕ is the porosity.

2.1.1. Poroelasticity. The poroelasticity rate of strain $\dot{\varepsilon}^{el}_{ii'}$ is written in terms of stress tensor σ, pressure p of the wetting phase, and rock texture Θ via

$$\dot{\varepsilon}^{el}_{ii'kl} = C^{-1}_{ii'kl}(\Theta)\frac{D}{Dt}\left(\sigma_{kl} + \alpha(\Theta)p\delta_{kl}\right) \tag{7}$$

for fourth rank poroelasticity tensor $C_{ii'kl}$ and effective stress coefficient α. D/Dt represents a material time derivative measuring the rate of change of a tensor in time with respect to a local reference frame fixed to a translating, rotating material volume element. The texture Θ represents a set of variables characterizing the mineralogy, shape, size, orientation, and packing of the grains as well as fracture network properties. The elastic coefficient (bulk and shear moduli of the drained porous medium) and the effective stress coefficient of the porous medium are calculated in terms of the composition, porosity, and mineral elastic properties using *Berryman*'s [1980, 1986] approach and corrected for the presence of fractures [*Budiansky and O'Connell,* 1976; *O'Connell and Budiansky,* 1977].

2.1.2. Viscosity. The viscoplastic contribution $\dot{\varepsilon}$ is cast in the present approach as a nonlinear viscosity law in the form [*Tuncay et al.*, 2000a, 2000b, 2000c]

$$\dot{\varepsilon}^{vp}_{ii'} = \eta^{-1}_{ii'kl}\left(\sigma_{kl} + \tilde{\alpha}p\delta_{kl}\right). \tag{8}$$

The fourth rank viscosity tensor η depends on stress, wetting fluid pressure and texture [*Tuncay et al.*, 2000a]. The second term in the effective stress involves a coefficient $\tilde{\alpha}$ that is usually taken in the literature to be unity. The shear viscosity is assumed to depend on texture [*Tuncay et al.*, 2000a, 2000c].

The texture dependence of the viscosities is not well characterized. A simple approach is the approximation of viscosities as a function of grain size and porosity. For example,

$$\mu = A\exp(-\phi/B\phi_0)^n g(r)\Gamma^p , \tag{9}$$

where A, B, a, b, and n are material properties, $g(r)$ is $e^{a+b\ln r}$ (a correction for grain size r), and ϕ is porosity. We have introduced a measure Γ of rock competency that accounts for the degree to which grains are attached to each other [*Tuncay et al.*, 2000c]. The equation for Γ is taken in the form

$$\frac{D\Gamma}{Dt} = R(\Gamma,F) . \tag{10}$$

Here F is a failure function that depends on macroscopic stress, wetting fluid pressure, rock texture, and mineralogy. The dynamics

of Γ is relatively fast so that its evolution is closely related to the curve $R(\Gamma,F)=0$ [*Tuncay et al.*, 2000c]. The Γ dynamics is, in a sense, a cooperative phenomenon: a decrease in competence fosters more rapid Γ decline. The failure function F is assumed to take the form [*Drüker-Prager and Prager*, 1952]

$$F = hJ_1 + \sqrt{J_2} - c, \tag{11}$$

where J_1 is the first invariant of the effective stress tensor and J_2 is the second invariant of the deviatoric stress tensor. The parameters h and c can be represented in terms of friction angle and cohesion determined from conventional triaxial compression experiments [*Desai and Siriwardane*, 1984]. In this study, we focus on the coupling between salt motion, multiphase flow, and sedimentation. Therefore we use a relatively high rock strength to avoid faulting. Faults associated with salt motion will be pursued in a future study. The parameter p in (9) is taken as equal to 1 and 6 for bulk and shear viscosity expressions, respectively.

2.1.3. Fracturing. As the present theory is macroscopic, the variables describing fractures are considered to be part of the texture Θ. This assumes that the length scale on which the phenomena of interest vary is much greater than the fracture length or interfracture spacing. Otherwise, one must treat fractures individually, an approach that is not viable for basin-scale modeling.

The dynamics of the fracture network in our model is based on a statistical representation. For example, consider a set of fractures of length L with normal $\mathbf{n}$ for a three-dimensional spectrum of normal orientations. Then the rate of change for L in the rock-fixed frame takes the form

$$\frac{dL}{dt} = R(p,\Theta,\sigma), \tag{12}$$

where the fracture extension rate R depends on the normal stress σ, the wetting phase fluid pressure p, and the texture Θ of the surrounding rock (including fracture length and aperture). A similar equation for the fracture aperture is developed. The parameters used in (2) are given by *Tuncay et al.* [2000b].

Let f' be the number density of sites at which fractures may nucleate. By definition of the undeformed state, $f'=f$, but f' can differ from f due to changes in rock texture from diagenesis or mechanical processes. In the simplest case where fracture nucleation sites are not created or destroyed, f' obeys the conservation equation $\partial f'/\partial t + \nabla\cdot(f'\mathbf{u}) = 0$. In a macrovolume element of volume V, there are Vf' fracture nuclei and hence a fracture void space $Vf'\pi r^2 a$, where a and r are the aperture and radius of the assumed penny-shaped fractures, respectively. To compute the dilatation, we focus on a fixed volume V_m of solids and follow its change in a time δt. The volume of the unfractured rock V_{unfr} is related to V_m and the porosity ϕ_m of the unfractured rock via $V_{unfr} = V_m + \phi_m V_{unfr}$. Hence $V_{unfr} = V_m/(1-\phi_m)$. Note that total porosity is equal to $\phi = \phi_m + \phi_{fr}$. The total volume V of the sample of rock containing V_m is then

$$V = (1-\phi_m)^{-1} V_m + V\Delta, \tag{13}$$

where $\Delta = f'\pi L^2 a$. With this, the volume of rock $V(t)$ at time t for fixed volume of solids V_m (considered incompressible and not to expand thermally or react) is given by

$$V(t) = V_m(1-\phi_m)^{-1}(1-\Delta). \tag{14}$$

Noting that

$$tr\dot{\varepsilon}^{fr}_{ii'} = \lim_{\delta t\to 0} \frac{V(t+\delta t) - V(t)}{V(t)\,\delta t}, \tag{15}$$

one obtains

$$tr\dot{\varepsilon}^{fr}_{ii'} = [1-\Delta]^{-1}\frac{D\Delta}{Dt}, \tag{16}$$

where D/Dt is the material derivative, i.e., the derivative in the reference frame fixed to the solids.

The tensor character of the fracture-mediated deformation is related to the directions of each fracture through its normal $\mathbf{n}$ to the fracture plane. Consider the expression

$$\dot{\varepsilon}^{fr}_{ii'} = [1-\Delta]^{-1}\frac{D}{Dt}(\Delta n_i n_{i'}). \tag{17}$$

Here D/Dt represents a material time derivative; however, now it also must account for the rotation of the fracture normals as they change direction with flexure, shearing, or other deformation. Note that the trace of this expression agrees with the earlier result for the dilatation. Finally, this expression agrees with simple cases wherein all fractures are parallel.

In our model a finite (but representative) number of fracture orientations is accounted for. We use the fracture kinetics formulation of *Ortoleva* [1994a] and *Sonnenthal and Ortoleva* [1994]. However, here we replace the least compressive stress in the formulation by the stress component normal to each fracture plane. This allows calculation of fracture length and aperture for each fracture orientation. For example (if we assume that only vertical fractures can occur as for a one-dimensional problem), since the stress component normal to any vertical plane is the same because of the symmetry, an isotropic fracture network develops. In three-dimensional problems our proposed algorithm has the power to predict a complex fracture network with preferential orientations dictated by the structure of the stress tensor.

Since the fracture network is well defined, the anisotropic fracture permeability can be calculated approximately. The anisotropic fracture permeability of a fracture network consisting of a single fracture orientation is given by

$$K^{fr}_{ii'} = \lambda(\delta_{ii'} - n_i n_{i'}), \tag{18}$$

where $\mathbf{n}$ is the unit normal to the fracture plane and $K^{fr}_{ii'}$ is the fracture permeability. The parameter λ can be approximated by

$$\lambda = \beta\phi_{fr}\frac{a^2}{12}. \tag{19}$$

Here β is a factor accounting for the connectivity of fractures. For large fracture lengths and dense networks, β approaches unity, whereas for small fracture lengths and low fracture densities it vanishes. A discussion of this factor is given by *Oda* [1985, 1986]. In this study, β is taken as unity. We assume that the total fracture permeability is obtained by summation of fracture permeabilities for all orientations and statistical classes multiplied by the fracture porosity which has been proposed previously by *Chen et al.* [1999]. It is assumed that fluid flow is slow and the disturbance at fracture intersections is negligible. We refer to *Tuncay et al.* [2000b] for further details.

2.2. Multiphase Flow

Conservation of mass for fluid species yields the basic framework for the analysis of multiphase reaction-transport phenomena. Let $c_{\alpha i}$ be the concentration of species α in phase i ($\alpha = 1,2,\cdots N$; $i=1,2,\cdots N_p$) and s_i be the saturation (volume fraction) of pore space occupied by phase i. Conservation of mass for α in i yields

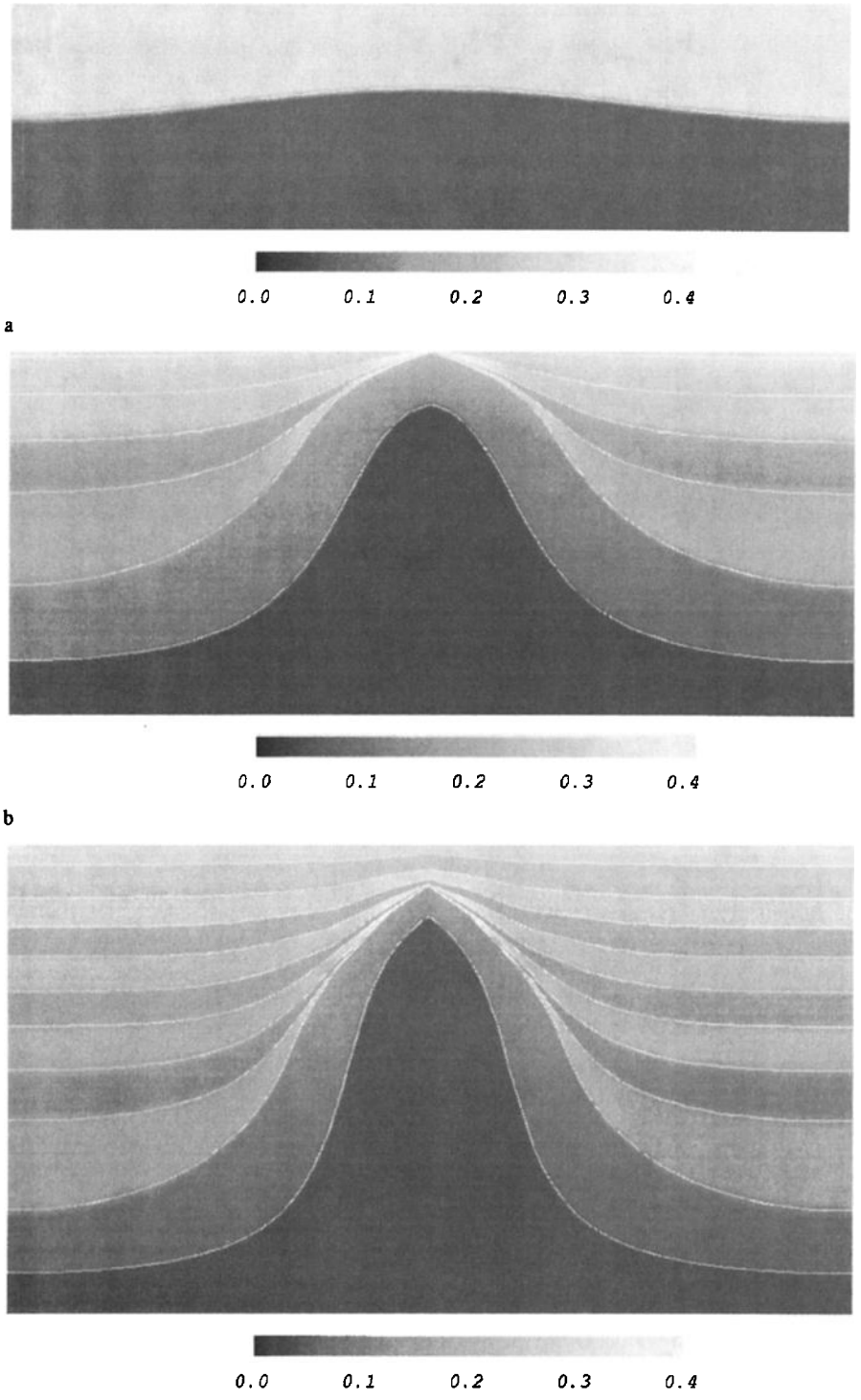

Figure 1. Porosity distribution (indicated by shading) at (a) $t=0$, (b) $t=4.2$, and (c) $t=8.8$ Myr into the simulation showing alternating sandstones and shales, the lowest layer being salt. Note the enhanced porosity associated with fracturing at the tip of the wave.

$$\frac{\partial \phi s_i c_{\alpha i}}{\partial t} = -\nabla \cdot \mathbf{J}_{\alpha i} + R_{\alpha i}, \tag{20}$$

where $\mathbf{J}_{\alpha i}$ is the vector flux of α in i (moles/rock area time) and $R_{\alpha i}$ is the moles of α created in i per volume of phase i. Interphase exchange cannot affect the total number of moles of a species per rock volume. Thus, summing (20) over all phases ($i=1,2,\cdots N_p$) yields the sum equations

$$\frac{\partial \phi c_\alpha}{\partial t} = -\nabla \cdot \mathbf{J}_\alpha + R_\alpha \tag{21}$$

$$c_\alpha = \sum_{i=1}^{N_p} s_i c_{\alpha i}, \tag{22}$$

$$\mathbf{J}_\alpha = \sum_{i=1}^{N_p} \mathbf{J}_{\alpha i}, \tag{23}$$

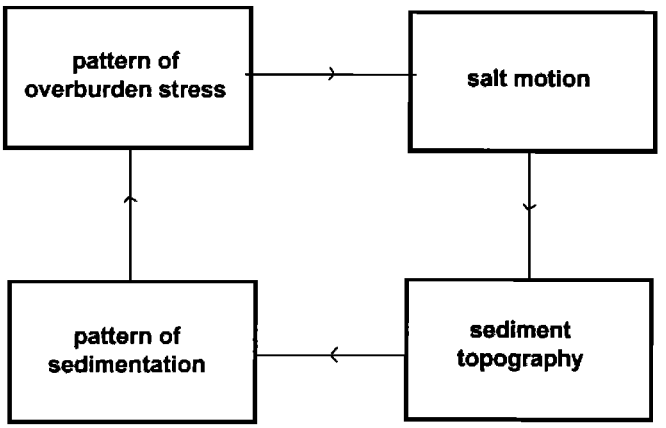

Figure 2. The feedback between salt motion and sedimentation underlies the salt diapirism instability.

$$R_\alpha = \sum_{i=1}^{N_p} R_{\alpha i}. \tag{24}$$

The reduced set of sum phase conservation equations is supplemented with the set of phase exchange equilibrium conditions [see *Ortoleva*, 1998, and references cited therein]:

$$\mu_{\alpha i} = \mu_{\alpha j}, \tag{25}$$

for all phases i and j. Here $\mu_{\alpha i}$ is the chemical potential of species α in phase i. The flux term is approximated by

$$\mathbf{J}_{\alpha i} = \phi s_i c_{\alpha i} \mathbf{v}_i - \phi s_i D_{\alpha i} \nabla c_{\alpha i}, \tag{26}$$

where $\mathbf{v}_i$ is the velocity of fluid phase i. The last term in (26) represents the effect of diffusive/dispersive transport, $D_{\alpha i}$ being the diffusion/dispersion tensor. The multiphase flow is assumed to follow the generalized Darcy law. The geometry of the phases in the pores is assumed to be describable in terms of the saturations. Then the black oil model is written

$$\phi s_i (\mathbf{v}_i - \mathbf{u}) = -\frac{\kappa \kappa_i}{\mu_i} (\nabla p_i + g \rho_i^m \mathbf{z}), \tag{27}$$

where κ is the single-phase permeability, κ_i is the relative permeability of phase i, g is the gravitational acceleration, ρ_i^m is the mass density of fluid phase i, and $\mathbf{z}$ is the unit upward pointing vector. The relative permeability curves are approximated by

$$\begin{cases} 0, & s_i < s_{ir}, \\ \left(\dfrac{s_i - s_{ir}}{s_{im} - s_{ir}} \right)^m, & s_i > s_{ir}, \end{cases} \tag{28}$$

where s_{r1} is the saturation when phase m is immobile. Parameters s_{r1} and m depend on texture. It is expected that s_{im} and m are bigger for small grain size and low-porosity medium.

This flux law is supplemented by a mechanical equilibrium condition.

$$p_i = p_{i'} + \Pi_{ii'}, \tag{29}$$

relating the fluid pressures in phases i and i' by the capillary pressure $\Pi_{ii'} = \Pi_{ii'}(s_1, s_2, \cdots s_{N_p}, \Theta)$. *Van Genuchten*'s [1980] expression is used to approximate the capillary pressure function:

$$\frac{s_1 - s_{r1}}{s_{m1} - s_{r1}} = \left[1 + \left(\frac{\alpha \Pi_{12}}{100} \right)^n \right]^{-1-1/n}, \tag{30}$$

where subscript 1 refers to water phase, s_{r1} is the irreducible water saturation, s_{m1} is the upper limit of water saturation, and α and n are material properties. The unit of capillary pressure given is pascals. The equations are completed with a set of state equations $\rho_i(c,T)$. For a two-phase oil-water system we use state expressions in the form of

$$\rho_i = \rho_i^0 \left[1 + \frac{p_i - p_0}{K_i} - \alpha (T - T_0) \right], \tag{31}$$

where ρ_i^0 is the reference density, p_0 is the reference pressure (1 atm), T_0 is the reference temperature, K_i is the bulk modulus, and α is the thermal expansivity.

2.3. Remarks

In addition to the coupling of deformation to other phenomena through the incremental stress formulation, there are numerous indi-

Table 1. Model Parameters Used in the Simulations

	Halite	Quartz	Muscovite
Salt body composition	100	0	0
Shale composition	0	0	100
Sandstone composition	0	100	0
Grain size, mm	0.01	0.05	0.01
Density, g/cm^3	2.0	2.7	2.7
Bulk modulus, GPa	80	85	70
Shear modulus, GPa	10	37	28
A (bulk), Pa·sec	1.57x10^{26}	1.57x10^{26}	1.57x10x^{26}
B (bulk), Pa·sec (equation (9))	0.329	0.108	0.111
n (bulk) (equation (9))	1.	1.	1.
A (shear), Pa·sec (equation (9))	3x10^{18}	3.15x10^{25}	1.57x10^{25}
B (shear) (equation (9))	0.38	0.204	0.21
n (shear) (equation (9))	1.	1.4	1.4
ϕ_0 (equation (9))	0.05	0.4	0.4
a (equation (9))	0.6	0.6	0.6
b (equation (9))	0.739	0.739	0.739

Table 2. Flow Parameters Used in the Simulations

	Halite	Quartz	Muscovite
Irreducible water saturation (equation (28))	0.5	0.2	0.4
m (equation (28))	3	3	3
n (equation (30))	4	3	4
α (equation (30))	0.020	0.040	0.020
	Water	**Oil**	
Reference density	1.025	0.80	
Bulk modulus, GPa	2.0	1.5	
Viscosity, Pa·sec	0.001	0.0008	

rect couplings. For example, rock properties such as permeability, multiphase flow parameters, reactive grain surface area, and thermal conductivity depend strongly on texture. As the latter is affected by stress and deformation, a complex network of coupling relations is thereby expressed. For further discussion of the consequence of this network, see *Ortoleva* [1994a, 1994b, 1998], *Tuncay et al.* [2000a, 2000b], and *Dewers and Ortoleva* [1994a, 1994b].

The unity brought about by the above approach gives our modeling the generality needed to solve many salt tectonic problems. Salt responds differently than sediments simply because its mineralogy is NaCl and other salts, and not quartz, clays, or carbonates. Various lithologies differ among themselves due to the porosity, grain size, and mineralogy. Similarly, salt has relatively low viscosity and hence large least compressive effective stress, thereby repressing fracturing there (as the latter nucleate and grow in low compressive stress regimes).

The final set of equations includes the total momentum balance equation (4), momentum balance equations for the fluid phases (27), mass balance equation for the solid phase (6), and mass balance equations for the fluid species (21). The total momentum balance is solved coupled to the incremental stress rheology accounting for poroelasticity, viscosity, and fracturing. (12) and a similar equation for fracture aperture are solved for all fracture orientations. The rate of strain due to fracturing is used to account for the coupling between stress and fracturing. The anisotropic fracture permeability tensor is employed in the solution of flow equations. The sedimentation rate is modified based on the velocity of the surface using the expression

$$S^*(x,y,t) = S(t) + \dot{z}(x,y,t) - \dot{z}_0(t), \tag{32}$$

where $S(t)$ is the sedimentation rate which is assumed to be independent of position for planar surfaces, $\dot{z}(x,y)$ is the velocity of the surface, and $\dot{z}_0$ is the average velocity of the surface.

3. Sedimentation-Salt Tectonic and Other Feedback Mechanisms

It is believed that the coupling between salt motion-induced sediment topography and the distribution of sedimentation is key to determining salt morphology as well as the geometry of neighboring sediment bodies. We suggest that this dynamic should be viewed as self-organization. If a rising diapir causes a bump in the shape of the top surface of the sediment pile, additional sediment will tend to deposit on the flanks of the bump. This sediment will then tend to squeeze more of the (relatively light) salt into the diapir, causing it to rise further. If this dynamic continues, the diapir will have sustained growth (see Figure 1). If the tip of the salt diapir is too far below the surface of the sediment, then this coupling is diminished so that there is a limited depth range for the operation of this mechanism.

The general theme is as follows. The distribution of sedimentation rate is a functional of the shape of the top of the sediment pile. The local sedimentation rate determines the local overburden on the salt and hence promotes salt withdrawal and its injection into the diapir. The resulting feedback is summarized in Figure 2. If the salt and sediment are both perfectly horizontal, this feedback is not operating. Thus it seems that even the smallest departure from planarity can trigger diapirism. Some caution is required, however, in that there may be a critical amplitude below which there is no diapiric response. Thus diapirism emerges as a symmetry-breaking instability of the planar state, a theme common to other patterning phenomena in chemical and physical systems [*Nicolis and Prigogine,* 1977; *Ortoleva,* 1992] and geological systems [*Nicolis and Nicolis,* 1987; *Ortoleva et al.,* 1987a, 1987b; *Ortoleva,* 1990; *Haase et al.,* 1980].

The specific algorithm used in our simulator is as follows. The system is fed a spatial average amount of sediment per year (say 200 m/Myr of alternating, equally thick shale and sandstone precursor sediments). However, the local rate of sedimentation is computed in a given computational time step so as to eliminate any putative departure from planarity of the topography induced by the diapirism and salt withdrawal (at the flanks of a diapir). Thus a local thinning overlying the salt layer is compensated by the augmented sedimentation rate so as to form a minibasin or other sediment accumulation.

The sedimentation to salt deformation dynamic is just one of a family of feedback processes operating in a salt tectonic province. Buoyancy of salt relative to compacted sediment also can drive an instability analogous to the Benard instability wherein overturning convection can emerge when a denser fluid overlies a lighter one [*Nicolis,* 1995; *Biot and Ode,* 1965; *Biot,* 1966]. The complex rheology of the rocks surrounding salt, however, may mask the pattern-forming process. For example, when horizontal salt/sediment layers are subject to an overall lateral extension, the pattern of locally induced failure in the overlying sediment can yield upward migration pathways for the salt that was otherwise trapped by an overlying competent and stiff layer of sediment. Similarly, salt diapirism can result from its complex interplay with buckling and failure instabilities as in a regime of lateral compression.

An overall sloping of the salt layer or an overall gradient in the rate of sedimentation (as from near offshore to farther out in the

Gulf of Mexico) can trigger salt diapirism. These larger spatial scale "perturbations" of the "perfect" horizontal state can trigger salt diapirism and other features on a scale much shorter than the overall region of the graded conditions. Such wavelength selection (i.e., the appearance of patterns on scales larger or smaller than that of the perturbation) is common in nonlinear dynamical systems. Such preferred scales of diapirism have implications for the size of salt minibasins and in the spacing of salt waves emerging in a sloped salt bed.

While one can speculate at length on these and other salt tectonic self-organization phenomena, the great number of strongly coupled processes underlying the dynamics of a salt province requires a quantitative analysis. After all, the behavior of salt systems is a reflection of the positive and negative interactions among these many factors. Thus we now address some of these issues via the quantitative modeling approach outlined above.

4. Numerical Approach

In this study we use the updated Lagrangian approach to solve the time-dependent large deformation problem for geological materials satisfying the incremental stress rheology [*Bathe et al.*, 1975; *Bathe*, 1996; *Tuncay et al.*, 2000a]. In our numerical approach, all variables are referred to an updated configuration in each time step. The approach has two major steps. First, the incremental stress rheology equations are solved at the integration points of the finite elements. Second, the displacements are computed by using a global deformation solver. At each time step, iterations of these two steps are performed until the norm of the change in displacements between two consecutive iterations is less than a specified tolerance. The two-step solution technique allows the introduction of new deformation processes with only minor changes in the code. We use the conjugate gradient iterative technique with a simple diagonal preconditioner to solve for the incremental displacements. The finite element code and iterative solver are parallelized. The details of the finite element formulation are provided by *Tuncay et al.* [2000a].

In the multiphase module the Galerkin-type finite element approximation is used for saturations, concentrations, and pressures. The nonlinear terms and boundary conditions are treated in a fully implicit manner. An upwinding method is developed and implemented in the multiphase module to stabilize the saturation fronts. The mass matrices are lumped to increase the stability as suggested in previous studies [*Huyakorn et al.*, 1994; *Abriola and Rathfelder*, 1993]. The computer model accommodates a wide variety of boundary conditions. Because of the highly nonlinear behavior of the equations a Newton-Raphson technique is employed to solve the nonlinear algebraic equations arising from the discritization.

The finite element grid accretes with sediment infilling. A new sediment layer is introduced when the sediment layer at the top of the basin reaches a critical thickness. In contrast, when erosion creates a top layer that is locally too thin, the finite element grid is locally reorganized to preserve numerical accuracy. This accreting, reorganizing grid that also adapts to sedimentary features as they are added is required to capture sedimentary detail and to insure numerical stability and accuracy.

The interaction of the top of the sediment pile with the overlying fluids (atmosphere or sea bottom) is accounted for by the value of normal stress and the (assumed) absence of tangential shear. The no-shear lateral boundary condition allows for natural compaction at the sides of the basin. Lateral compression/extension and subsidence/upheaval are imposed at the sides and bottom. The sides and bottom are assumed to be impermeable to fluid flow.

All computational modules are packaged in an overall structure that insures that all equations are satisfied at each time step. The time step is allowed to change to insure accuracy and computational efficiency.

5. Simulation Results

5.1. Two-Dimensional Salt Wave With Single Phase Flow

A number of two-dimensional simulations were carried out to gain insight into the interaction between salt migration, sedimenta-

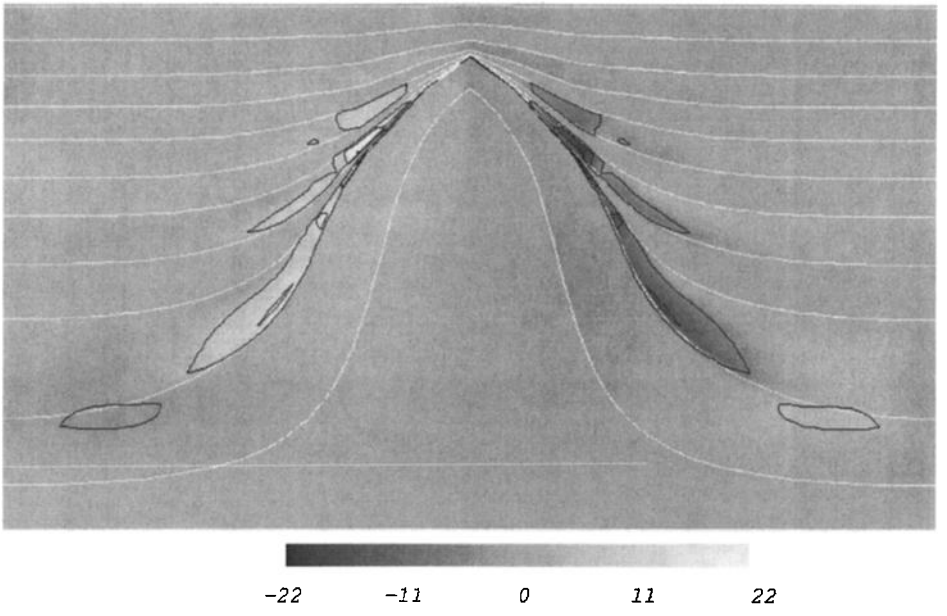

Figure 3. Overpressure distribution (bars) at (a) $t=1.46$, (b) $t=1.56$, and (c) $t=1.66$ Myr. The focus of overpressure moves upward along the flanks of the wave, indicating a migrating, fracture-associated compartment.

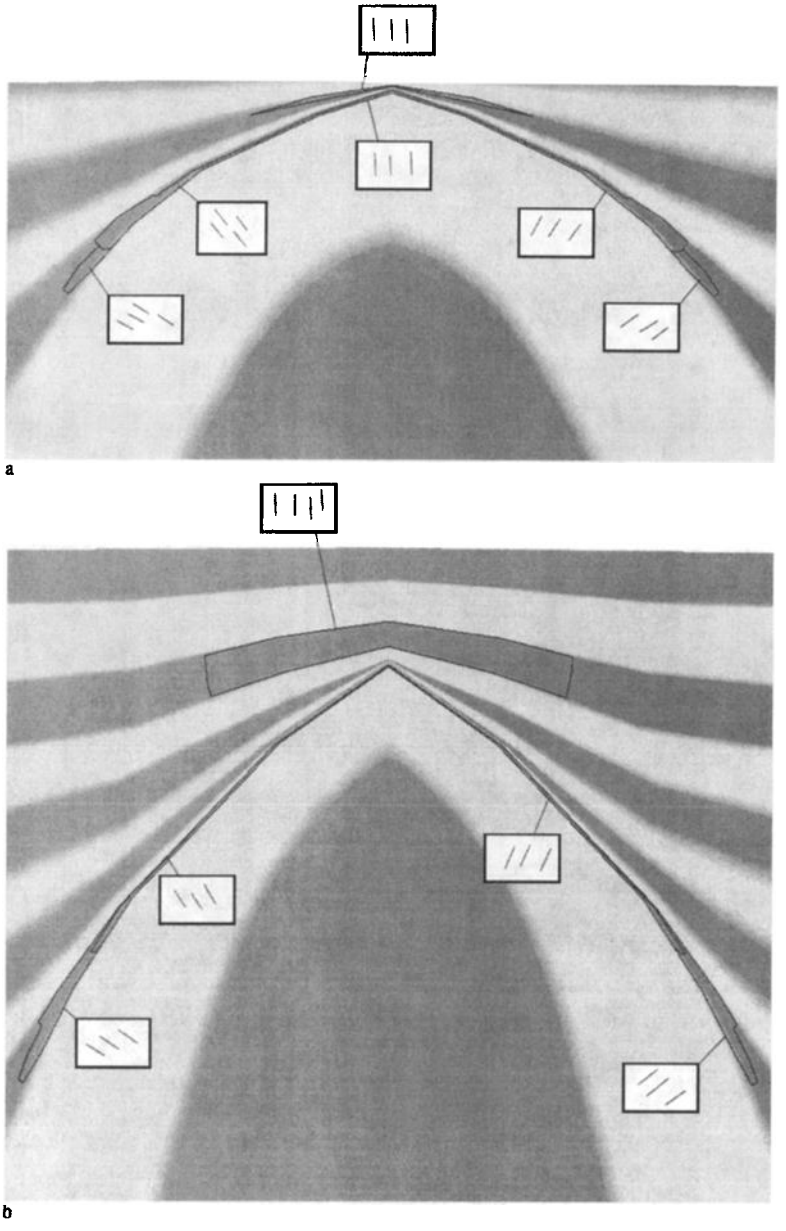

Figure 4. Oil saturation distribution at (a) $t=1.46$, (b) $t=1.56$, and (c) $t=1.66$ Myr. Gray level indicates the oil saturation. Note the fracture-assisted petroleum migration upward along the flanks of the wave.

tion, fracturing, and fluid flow. Since the boundary conditions are chosen to be symmetric (no vertical shear stress and no horizontal displacement at both sides), only simulation of a half salt wave is sufficient to study the dynamics of such systems. In two-dimensional simulations the number of finite elements starts from around 600 and increases with the addition of new elements from sedimentation to around 3000. The wavelength is taken as 10 km. Initially, the computational domain consists of a salt body underlying a shale layer. Then alternating layers of shales and sandstones are added. The sedimentation distribution is modified so that the top surface remains horizontal during evolution (i.e., putative topographic variations are filled in by sedimentation). The initial relief in the salt geometry is 400 m. The parameters used in the simulations are presented in Table 1 (grain size, rheologic parameters, density) and Table 2 (flow parameters). The time step was allowed to change in the simulations. In every time step, iterations are performed until the node coordinates, pressure, fracture properties, and stress tensor converge. If convergence is not achieved in ten iterations, the time step is reduced to half of its value. If convergence is achieved in two iterations, time step is increased by a factor of 1.10. It should be noted that these iterations correspond to outer loop iterations. Each computational module (such as stress/deformation, multiphase flow, fracture mechanics) has its own iteration loop and error criteria to accurately solve for the nonlinear governing equations.

In 8 Myr the salt relief reaches 3000 m in the example of Figure 1. In Figure 1, white lines indicate lithologic contacts. Contours are included in some of these figures to emphasis shading. Note the coevolving state of porosity. As the salt body moves upward, it pushes and extends the overlying sediments sideways, resulting in the reduction of least compressive stress and preservation of porosity. In our model porosity is solved from (6). Total porosity is given by the summation of matrix porosity and fracture porosity.

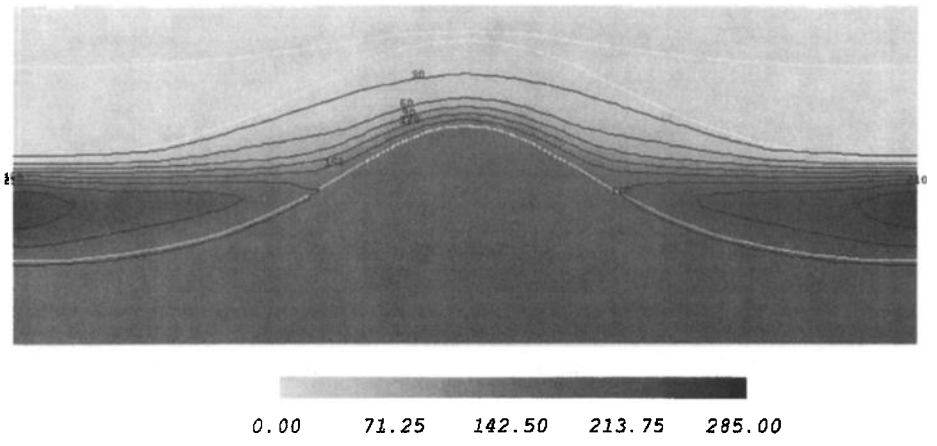

a

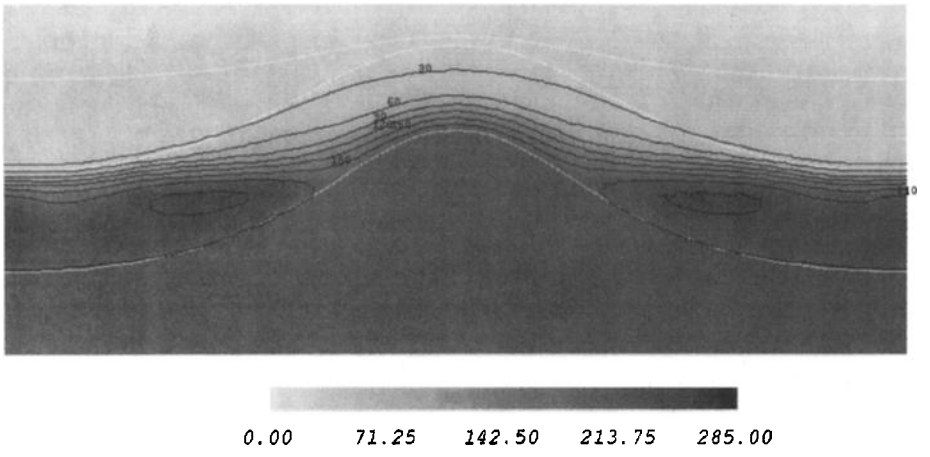

b

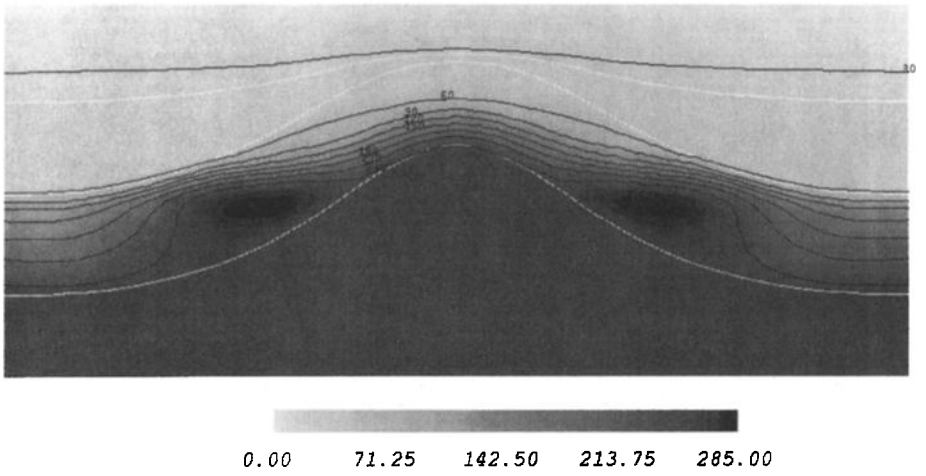

c

Figure 5. Shear stress distribution (MPa) at 8.8 Myr. Shear stress is indicated with shading and contour lines for emphasis. The white lines indicate the lithologic contacts.

Because of the feedback between the fracture mechanics and stress deformation through the volumetric rate of strain due to fracturing, the predicted porosity distribution accounts for both contributions. Salt motion significantly changes the sedimentation distribution resulting in very thin draped layers on top of the salt wave. As the salt motion slows down, the nonuniformity in layer thickness reduces, and eventually, the wave stalls.

Figure 3 illustrates the tendency of high-viscosity sandstones to resist deformation and to experience high shear stress. The shear stress in sandstones alters the least compressive stress orientation

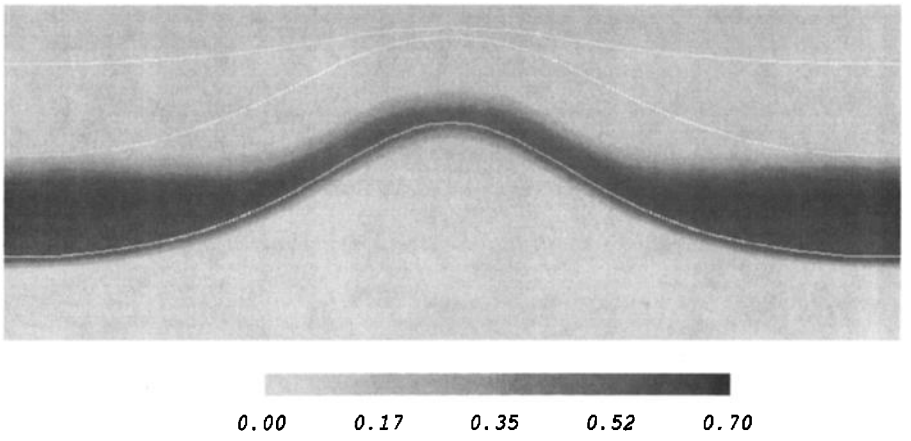

a

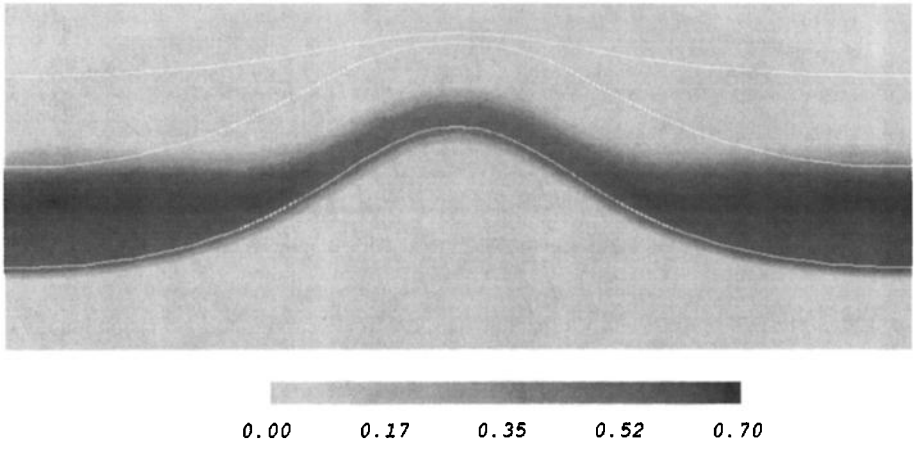

b

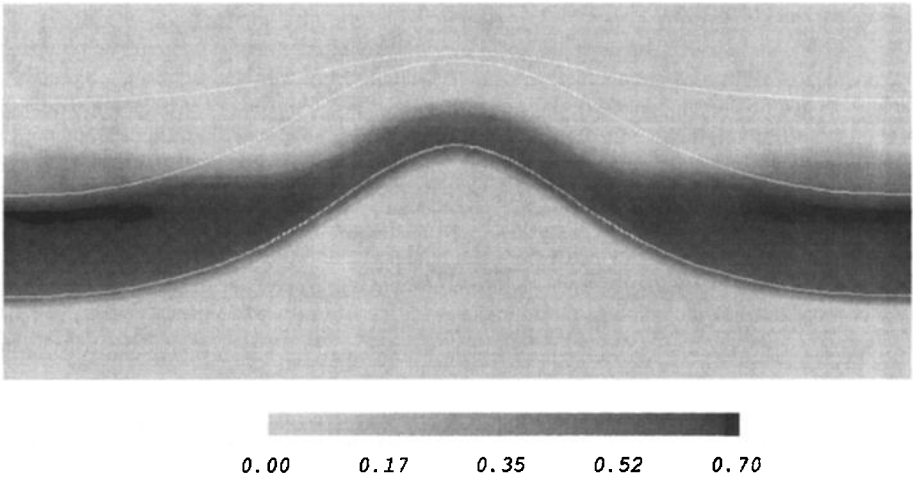

c

Figure 6. Dominant fracture orientations at (a) t=4.2 and (b) t=8.8 Myr. In this simulation, five fracture orientations were used. The solid line shows the border between different dominant fracture orientations.

there which, in turn, changes the fracture orientations. The evolution of dominant fracture orientation is demonstrated in Figure 4. Initially, fractures are essentially vertical. As the slope of the upper surface of the flanks of the salt body gets steeper, the dominant fracture orientations rotate, keeping essentially normal to the salt body. Because of their relatively high brittleness, only the sandstones fracture in this simulation, showing the lithologic control on the stress regime and fracture mechanics. Tensile fractures in rocks are the result of high fluid pressure (through the effective stress principle) and/or geometric effects such as bending and twisting. Depending

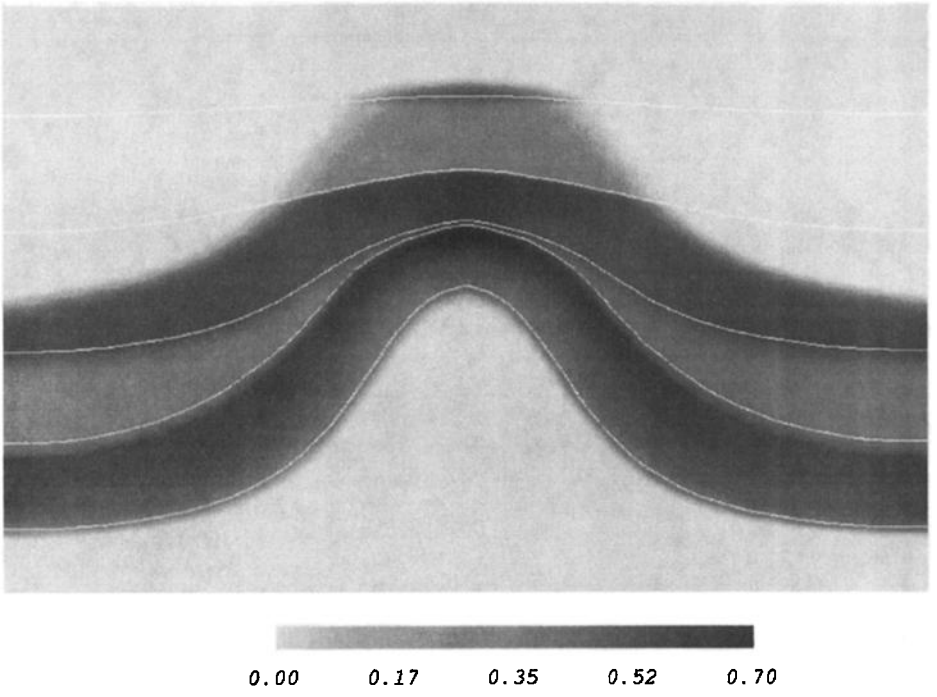

Figure 7. Oil saturation distribution at 3.76 Myr into the simulation.

on the rate of pressuring and mechanical properties, fracturing may occur as pressure increases. For example, shales that would not fracture under hydrostatic pressure can experience fracturing as a result of high overpressuring due to volume-increasing reactions or temperature increase. However, if the overpressure is dissipated through fluid flow, these fractures may heal because of the relatively low shear viscosity of shales.

5.2. Two-Dimensional Salt Wave With Multiphase Flow

To predict salt tectonics-related petroleum pools, one must coevolve petroleum generation/expulsion/migration with salt and rock deformation. In this simulation, the lower half of the shale overlying the salt body is assumed to be source rock. Figures 5 and 6 show the overpressure and oil saturation distribution as the oil is expelled into the overlying sandstone. As the oil migrates an overpressured compartment is created that moves upward along the shale toward the crest of the salt wave in coordination with the oil pool. Figure 7 shows the distribution of oil saturation after 3.76 Myr. The high permeability due to the high porosity and presence of fractures toward the top of salt body provides a pathway for multiphase fluid flow and related upward escape (seepage).

5.3. Two-Dimensional Salt Lens With Multiphase Flow

Low-permeability salt bodies form very efficient seals. In this simulation the salt body is laterally discontinuous and resides above shale. The lower half of the shale is assumed to be source rock. As the salt body moves upward, it drags the underlying shale layer. Because of the low permeability of salt, fluid can only flow around the salt body, resulting in high overpressure at the center, which in turn decreases the effective stress there. Figures 8 and 9 show the overpressure and porosity distributions after 5.56 Myr. The porosity and permeability beneath the edge of the salt lens become lower, completing the seal for the compartment. The high porosity at the center is a result of fracturing, the relatively low trace of the effec-

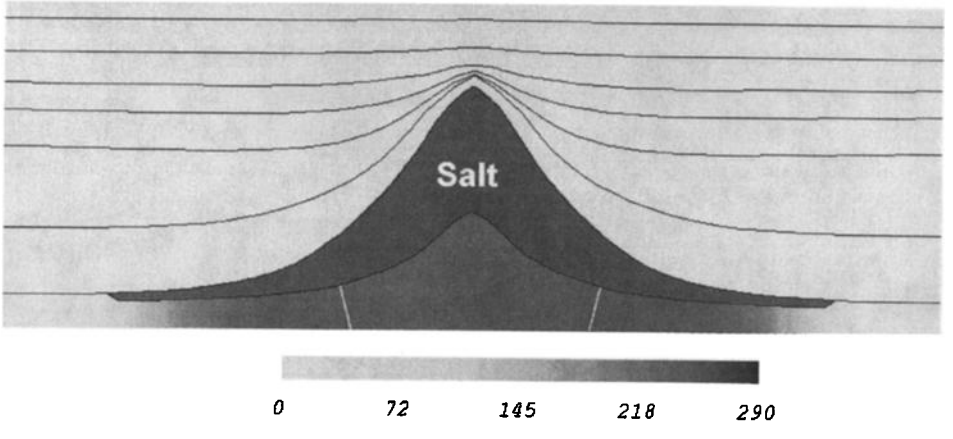

Figure 8. Overpressure (bars) distribution 5.56 Myr into the simulation.

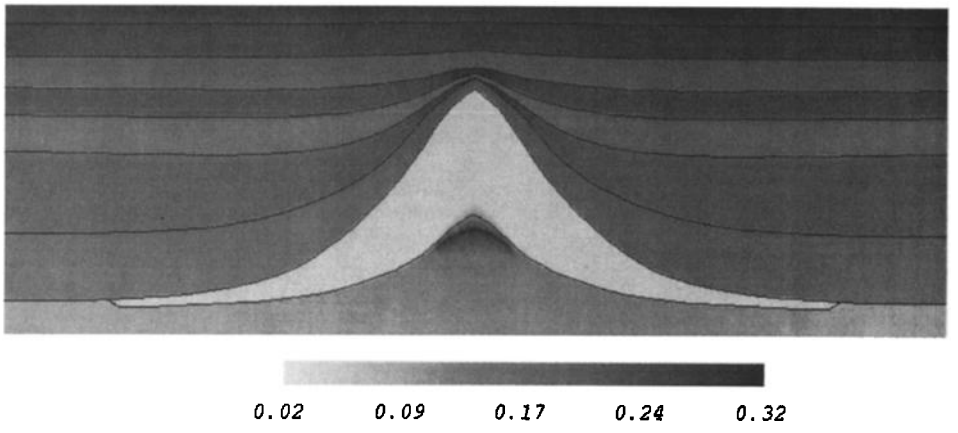

Figure 9. Porosity distribution at 5.56 Myr into the simulation.

tive stress tensor, and the consequent reduction of the compaction rate. Oil saturation history is shown in Figure 10. Although some oil leaks into the overlying shale layer, most of the oil is kept in the compartment. Within the domed shale underlying the salt there is fracture-assisted expulsion from the lower half of the shale (source rock) to the upper half. Overpressure is highest at the flow neutral boundary and flow is away from that boundary. The flow neutral boundary is created by the interplay of compaction and salt-induced stresses and other factors. This simple example demonstrates that a wide range of possibilities might arise in the case of source rock beneath the salt body as a result of salt motion and associated overpressuring. In the presence of a seal such as salt bodies, overpressured or underpressured zones may affect the rock rheology in a number of ways. As pressure increases, the first term in the failure criterion (equation (11)) reduces, decreasing the required deviatoric stress to fail the rock. Such weak zones may alter and guide the salt motion.

6. Conclusions

The myriad of salt tectonic phenomena can be understood within the unifying framework of the theory of self-organizing system. The state of a horizontal, planar salt bed placed in a basin of similarly configured sedimentary beds is unstable due to the density difference between salt and sedimentary rocks. A variety of situations can trigger the inherent instability of such a system including (1) a local topographic feature in the original salt bed, (2) lateral nonuniformity in the sediments associated with their mass density and resulting nonuniform loading, (3) local thermal anomalies and the induced nonuni-

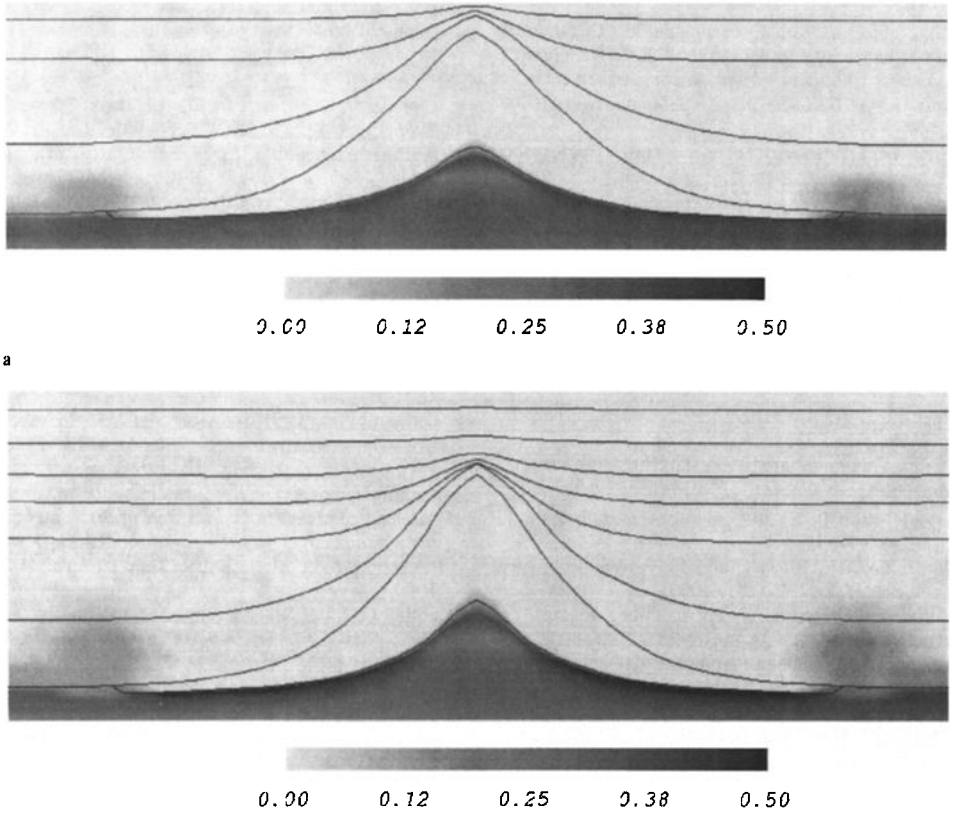

Figure 10. Oil saturation distribution at (a) t=3.12 and (b) t=5.56 Myr.

formity in compaction rate, diagenesis, or organic reactions in the salt adjacent sediments, (4) deeper-lying tectonic activity (notably faulting), (5) basin extension/compression and the associated creation of local rock failure and buckling, and (6) lateral nonuniformity in the rate or texture of sedimentation. Once these processes trigger the growth of a diapir, wave, or other feature, the feedback processes as in Figure 2 and others involving the many operating basin RTM processes can accelerate the growth of these features.

Because of the many competing tendencies, many factors bear on the possibility and extent of salt morphological development. Thus there is a complex zoning in the many-dimensional space of these factors in which various salt tectonic features can develop.

To unravel this complexity in a quantitative and rational manner and to model particular basins, one needs a comprehensive RTM model. We believe that the present model is a step forward in achieving that level of predictability and for deriving practical implications for petroleum exploration and production. It is expected that further research on fracturing and failure descriptions and associated rate laws as well as irreversible deformation of multimineral rocks will greatly enhance such RTM models.

Acknowledgments: This work has greatly benefited from conversations with and assistance from A. Park, K. Sundberg, D. Payne, W. Sibo, and J. Golding. This work was supported by a contract with the Gas Research Institute. We would like to thank two anonymous reviewers and the Associate Editor Ctirad Matyska, whose suggestions improved the manuscript.

References

Abriola, L.M., and K. Rathfelder, Mass balance errors in modeling two-phase immiscible flows: causes and remedies, *Ad. Porous Media, 16*, 223-239, 1993.

Aubertin, M., S. Servant, and D.E. Gill, Experimental identification of kinematic and isotropic hardening in rocksalt, in *Rock Mechanics Models and Measurements: Challenges from Industry*, edited by P.P. Nelson and S.E. Laubach, pp. 723-730, A. A. Balkema, Brookfield, Vt., 1994.

Bathe, K.J., *Finite Element Procedures*, Prentice-Hall, Englewood Cliffs, N. J., 1996.

Bathe, K.J., E. Ramm, and E.L. Wilson, Finite element formulations for large deformation dynamic analysis, *Int. J. Numer. Methods Eng., 9*, 353-386, 1975.

Berryman, J. G., Long-wavelength propagation in composite elastic media, I, Spherical inclusions, *J. Acoust. Soc. Am., 68*, 1809-1819, 1980.

Berryman, J. G., Effective medium approximation for elastic constants of porous solids with microscopic heterogeneity, *J. Appl. Phys., 59*, 1136-1140, 1986.

Biot, M.A., Three dimensional gravity instability derived from two-dimensional solutions. *Geophysics, 31*, 153-166, 1966.

Biot, M.A., and H. Ode, Theory of gravity instability with variable overburden and compaction. *Geophysics, 30*, 213-227, 1965.

Budiansky, B., and R. J. O'Connell, Elastic moduli of a cracked solid, *Int. J. Solids Struct., 12*, 81-97, 1976.

Carter, N.L., S.T. Horseman, J.E. Russell, and J. Haydin, Rheology of rocksalt, *J. Struct. Geol., 15*, 1257-1271, 1993.

Chen, M., M. Bai, and J.-C. Roegiers, Permeability tensors of anisotropic fracture networks, *Math. Geol., 31*, 355-373, 1999.

Cobbold, P. R. (Ed.), New insights into salt tectonics: Collection of invited papers reflecting the recent developments in the field of salt tectonics, *Tectonophysics, 228*, 141-445, 1993.

Daudre, B., and S. Cloetingh, Numerical modeling of salt diapirism: Influence of the tectonic regime, *Tectonophysics, 240*, 59-79, 1994.

De Las Cuevas, C., Pore structure characterization in rock salt, *Eng. Geol., 47*, 17-30, 1997.

Desai, C.S., and H.J. Siriwardane, *Constitutive Laws for Engineering Materials*, Prentice-Hall, Englewoods Cliffs, N. J., 1984.

Dewers, T., and P. Ortoleva, Self-organization of mineralization patterns in metamorphic rocks through mechanochemical coupling, *J. Phys. Chem., 93*, 2842-2848, 1989.

Dewers, T., and P. Ortoleva, Geochemical self-organization III: A mechano-chemical model of metamorphic differentiation, *Am. J. Sci., 290*, 473-521, 1990a.

Dewers, T., and P. Ortoleva, A coupled reaction/transport/mechanical model for intergranular pressure solution, stylolites, and differential compaction and cementation in clean sandstones, *Geochim. Cosmochim. Acta, 54*, 1609-1625, 1990b.

Dewers, T., and P. Ortoleva, Differentiated structures arising from mechano-chemical feedback in stressed rocks, *Earth Sci. Rev., 29*, 283-298, 1990c.

Dewers, T., and P. Ortoleva, Interaction of reaction, mass transport, and rock deformation during diagenesis: Mathematical modeling intergranular pressure solution, stylolites, and differential compaction/cementation, in *Prediction of Reservoir Quality Through Chemical Modeling*, edited by I. Meshri and P. Ortoleva, *AAPG Mem. 49*, 147-160, 1990d.

Dewers, T., and P. Ortoleva, Non-linear dynamics in chemically compacting porous media, in *Modeling and Analysis of Diffusive and Advective Processes in Geosciences*, edited by W.E. Fitzgibbon and M.F. Wheeler, pp. 100-121, Soc. for Ind. and Appl. Math., Philadelphia, Pa., 1992.

Dewers, T., and P. Ortoleva, Formation of stylolites, marl/limestone alternations, and dissolution (clay) seams by unstable chemical compaction of argillaceous carbonates, in *Diagenesis IV, Dev. Sedimentol.* vol. 51, edited by K.H. Wolf and G.V. Chilingarian, pp. 155-216, Elsevier Sci., New York, 1994a.

Dewers, T., and P. Ortoleva, Nonlinear dynamical aspects of deep basin hydrology: Fluid compartment formation and episodic fluid release, *Am. J. Sci., 294*, 713-755, 1994b.

Drüker-Prager, D. C., and W. Prager, Soil mechanics and plastic analysis or limit design. *Q. Appl. Math., 10*, 157-165, 1952.

Ge, H., M.P.A. Jackson, and B.C. Vendeville, Kinematics and dynamics of salt tectonics driven by progradation, *AAPG Bull., 81*, 398-423, 1997.

Haase, S., J. Chadam, D. Feinn, and P. Ortoleva, Oscillatory zoning in plagioclase feldspar, *Science, 209*, 272-274, 1980.

Huyakorn, P.S., S. Panday, and Y.S. Wu, A three dimensional multiphase flow model for assessing NAPL contamination in porous and fractured media, I, Formulation, *J. Contam. Hydrol., 16*, 109-130, 1994.

Jackson, M.P.A., and C.J. Talbot, A glossary of salt tectonics, *Geol. Circ. 91-4*, Bur. of Econ. Geol., Austin, Tex., 1991.

Jackson, M.P.A., and B.C. Vendeville, Initiation of salt diapirism by regional extension: Global setting, structural style, and mechanical models, *Rep. Invest. 215*, Bur. of Econ. Geol., Austin, Tex., 1994.

Jackson, M.P.A., C.J. Talbot, and R.R. Cornelius, Centrifuge modeling of the effects of aggradation and progradation on syndepositional salt structures, *Rep. Invest. 173*, Bur. of Econ. Geol., Austin, Tex., 1988.

Jackson, M. P. A., and C. J. Talbot, External shapes, strain rates, and dynamics of salt structures, *Geol. Soc. Am. Bull., 97*, 305-323, 1986.

Koen, A. D., Subsalt play could rekindle outlook for Gulf of Mexico, *Oil Gas J., 91*, 23-26, 1993.

Mazariegos, R., M.J. Andrews, and J.E. Russell, Modeling the evolution of salt structures using nonlinear rocksalt flow laws, *Tectonophysics, 256*, 129-143, 1996.

Munson, D.E., and P.R. Dawson, Salt constitutive modeling using mechanism maps, in *Proceedings of First International Conference on the Mechanical Behavior of Salt*, edited by H.R. Hardy Jr. and M.L. Langer, pp. 717-737, Trans. Tech., Clausthal-Zelterfeld, Germany, 1984.

Nicolis, C., and G. Nicolis (Eds.), *Irreversible Phenomena and Dynamical Systems Analysis in Geosciences*, D. Reidel, Norwell, Mass., 1987.

Nicolis, G., *Introduction to Nonlinear Science*, Cambridge Univ. Press, New York, 1995.

Nicolis, G., and I. Prigogine, *Self-Organization in Nonequilibrium Systems*, John Wiley, New York, 1977.

O'Connell, R.J., and B. Budiansky, Viscoelastic properties of fluid-saturated cracked solids, *J. Geophys. Res., 82*, 5719-5735, 1977.

Oda, M., Permeability tensor for discontinous rock masses, *Geotechnique, 35*, 483-495, 1985.

Oda, M., An equivalent continuum model for coupled stress and fluid flow analysis in jointed rock masses, *Water Resour. Res.*, *22*, 1845-1856, 1986.

Ortoleva, P. (Ed.), Self-organization in geological systems: Proceedings of a Workshop held 26-30 June 1988, University of California at Santa Barbara, *Earth Sci. Rev.*, *29*(1-4), 417 pp., 1990.

Ortoleva, P., *Nonlinear Chemical Waves*, John Wiley, New York, 1992.

Ortoleva, P., *Geochemical Self-Organization*, Oxford Univ. Press, New York, 1994a.

Ortoleva, P. (Ed.), *Basin Compartments and Seals*, *AAPG Mem.*, *61*, 1994b.

Ortoleva, P., Basin compartment fundamentals, topical report Project GRI-97/0097), Gas Res. Inst., Chicago, Ill., 1998.

Ortoleva, P., E. Merino, J. Chadam, and C.H. Moore, Geochemical self-organization, I, Reaction-transport feedback mechanisms and modeling approach, *Am. J. Sci.*, *287*, 979-1007, 1987a.

Ortoleva, P., E. Merino, C.H. Moore, and J. Chadam, Geochemical self-organization, II, The reactive-infiltration instability, *Am. J. Sci.*, *287*, 1008-1040, 1987b.

Ortoleva, P., M. Maxwell, D. Payne, and W. Sibo, Naturally fractured reservoirs and compartments: A predictive basin modeling approach, in *Fractured Reservoirs: Characterization and Modeling, RMAG 1997 Guidebook*, edited by T.E. Hoak, A.L. Klawitter, and P.K. Blomquist, pp. 227-242, Rocky Mt. Assoc. of Geol., Denver. Colo., 1997.

Rice, J. R. 1975, Continuum mechanics and thermodynamics of plasticity in relation to microscale deformation mechanisms, in *Constitutive Equations in Plasticity*, edited by A.S. Argon, pp. 23-79, MIT Press, Cambridge, Mass., 1975.

Schultz-Ela, D.D., M.P.A. Jackson, and B.C. Vendeville, Mechanics of active diapirism, *Rep. Invest. 224*, Bur. of Econ. Geol., Austin, Tex., 1994.

Seni, S.J., and M.P.A. Jackson, Sedimentary record of cretaceous and tertiary salt movement, East Texas Basin, *Rep. Invest. 139*, Bur. of Econ. Geol., Austin, Tex., 1984.

Sonnenthal, E., and P. Ortoleva, Numerical simulations of overpressured compartments in sedimentary basins, in *Basin Compartments and Seals*, edited by P. Ortoleva, *AAPG Mem. 61*, 403-416, 1994.

Taylor, G., Salt theory undergoes revival, *AAPG Explor.*, *4*, 4, 14-15, 1995.

Tuncay, K., A. Park, and P. Ortoleva, Sedimentary basin deformation: An incremental stress approach, *Tectonophysics*, in press, 2000a.

Tuncay, K., A. Park, and P. Ortoleva, A forward model of three-dimensional fracture orientation and characteristics, *J. Geophys. Res.*, *105*, 16,719-16,735, 2000b.

Tuncay, K., A. Khalil, and P. Ortoleva, Failure, memory and cyclic fault movement, *Bull. Seismol. Soc. Am.*, in press, 2000c.

Tuncay, K., A. Park, D. Payne, and P. Ortoleva, 3-D fracture network dynamics in reservoirs, faults and salt tectonic systems, in *Fracture and In-Situ Characterization of Hydrocarbon Reservoirs*, Geol. Soc. London, in press, 2000d.

Turcotte, D. L., Fractals, chaos, self-organized criticality and tectonics, *Terra Nova, 4*, 4-12, 1992.

Van Genuchten, M.T., A closed form equation for predicting the hydraulic conductivity of unsaturated soils, *Soil Sci. Soc. Am. J.*, *44*, 892-898, 1980.

Van Keken, P.E., C.J. Spiers, A.P. van den Berg, and E.J. Muyzert, The effective viscosity of rocksalt: Implementation of steady-state creep laws in numerical models of salt diapirism, *Tectonophysics, 225*, 457-476, 1993.

Vendeville, B.C., and M.P.A. Jackson, The rise and fall of diapirs during thin-skinned extension, *Rep. Invest. 209*, Bur. of Econ. Geol., Austin, Tex., 1992.

Wawersik, W.R., Determination of steady state creep rates and activation parameters for rock salt, in *Measurement of Rock Properties at Elevated Pressures and Temperatures: A Symposium*, edited by H.J. Pincus and E.R. Hoskins, *ASTM Spec. Tech. Publ.*, *869*, 72-92, 1985.

Weijermars, R., M.P.A. Jackson, and B. Vendeville, Rheological and tectonic modeling of salt provinces, *Tectonophysics*, *217*, 143-174, 1993.

P. Ortoleva and K. Tuncay, Laboratory for Computational Geodynamics, Department of Chemistry, Chemistry Building, Indiana University, Bloomington, IN 47405. (ortoleva@indiana.edu; ktuncay@indiana.edu)

(Received July 7, 1999; revised February 29, 2000;
accepted March 29, 2000.)